DNA twist at high alkali ion concentrations: evidence against C-form DNA in solution

Koen R. Storm, Christian Wiebeler, Sergio Cruz-León, Caroline Körösy, Nadine Schwierz, Jan Lipfert

Angaben zur Veröffentlichung / Publication details:

Storm, Koen R., Christian Wiebeler, Sergio Cruz-León, Caroline Körösy, Nadine Schwierz, and Jan Lipfert. 2026. "DNA twist at high alkali ion concentrations: evidence against C-form DNA in solution." *Nucleic Acids Research* 54 (5): gkag192. https://doi.org/10.1093/nar/gkag192.

Nucleic Acids Research, 2026, **54**, gkag192
https://doi.org/10.1093/nar/gkag192
Molecular and Structural Biology

DNA twist at high alkali ion concentrations: evidence against C-form DNA in solution

Koen R. Storm [1,2,†], Christian Wiebeler [2,†], Sergio Cruz-León [3], Caroline Körösy [1,2], Nadine Schwierz [2,*], Jan Lipfert [1,2,*]

[1]Department of Physics and Debye Institute for Nanomaterials Science, Utrecht University, Princetonplein 1, 3584 CC Utrecht, The Netherlands
[2]Institute of Physics, University of Augsburg, Universitätsstrasse 1, D-86159 Augsburg, Germany
[3]Department of Theoretical Biophysics, Max Planck Institute of Biophysics, Max-von-Laue-Straße 3, D-60438 Frankfurt am Main, Germany

*To whom correspondence should be addressed. Email: Jan.Lipfert@uni-a.de
Correspondence may also be addressed to Nadine Schwierz. Email: Nadine.Schwierz@uni-a.de
†Koen R. Storm and Christian Wiebeler contibuted equally to this work.

Abstract

DNA is highly negatively charged, making its structure strongly dependent on the ionic environment. DNA twist—a central DNA property—varies with ion concentration and identity. Prior studies have focused on salt concentrations below 1 M, and it is unclear whether twist trends persist at higher concentrations. It has been proposed that at high salt, DNA transitions from its canonical B-form to C-form, originally observed by fiber diffraction. Here, we use single-molecule magnetic tweezers to measure DNA twist in high concentrations of LiCl, NaCl, KCl, and CsCl. For all salts, twist initially increases approximately as ~[salt]$^{1/2}$, but plateaus and even decreases above 3 M. LiCl causes the largest twist increase, by $\leq 0.9^\circ$ bp^{-1}, compared with physiological salt, still far below the suggested C-form values of 2–3° bp^{-1}. We perform extensive all-atom molecular dynamics simulations for DNA in LiCl solutions with different force fields. For parmbsc1, we observe good agreement with experiments when ion activities are taken into account. We find that simulations initiated in the C-form rapidly convert to the B-form, while the B-form remains stable. Our results demonstrate ion-specific, systematic changes in DNA twist beyond 1 M salt, but do not support a transition to the C-form for DNA

Graphical abstract

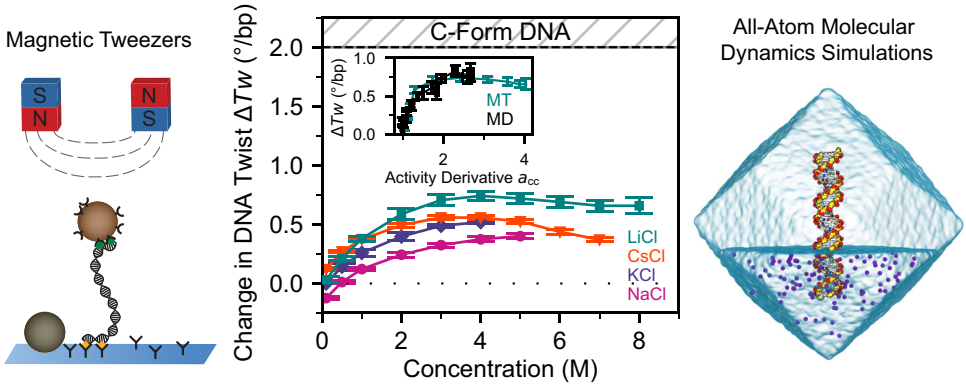

Introduction

DNA is the storage medium of all cellular life, and is increasingly used as a construction material in bionanotechnology. Since DNA is highly negatively charged, many of its properties depend sensitively on the ionic environment [1, 2]. In particular, the twist of the DNA helix, famously discovered by Watson and Crick [3], depends on the concentrations and type of ions in solution [4–7]. Initial measurements using a bulk assay with plasmid DNA found that DNA twist increases with increasing ion concentration and observed an approximately logarithmic dependence on ion concentration for monovalent ions in the range of 50–300 mM [4, 5]. More recent measurements using single-molecule magnetic tweezers (MTs) probed the changes in DNA twist up to a concentration of 1 M for all alkali ions [6–8]. The data reveal increasing DNA twist with increasing concentration following a power law dependence. While simple electrostatic theories predict the saturation of ionic effects at concentrations around 1 M monovalent salt [1], it is currently unclear whether and how the changes in twist continue above this concentration. Understanding DNA under conditions of high salt and low water activity [9] critically tests models of nucleic acid structure and of DNA–ion

Received: September 15, 2025. **Revised:** January 24, 2026. **Accepted:** February 16, 2026

interactions, which have typically been developed and tested only for lower concentrations. In addition, such conditions occur in halophiles, i.e. organisms that are exposed to extremely high salt conditions [10–13], such as *Halobacterium salinarum*, which grows best in 3–5 M monovalent salt [10]. In addition, high salt concentrations and ion-specific effects have been suggested to play critical roles in early life on earth [14–17].

In addition to ion concentration, ion identity also plays an important role. For Na^+, K^+, Rb^+, and Cs^+, the concentration dependencies of DNA twist follow very similar trends, and the twist at a given concentration increases with ion size. In contrast, Li^+ exhibits a stronger dependence on ion concentration than the other alkali ions and induces the largest absolute twist of all alkali ions. Molecular dynamics (MD) simulations complement these observations by providing atomic-level insight into DNA structure and dynamics. For example, they elucidate specific ion–DNA binding patterns, including the strong affinity of Li^+ for the phosphate groups of the DNA backbone, which underlies its pronounced effect on DNA twist and stiffness [6, 7, 18, 19]. However, the extent to which ion–DNA interactions continue beyond 1 M and affect DNA conformations is still not well understood.

Early work based on X-ray fiber diffraction suggested the existence of different conformational forms of double-stranded DNA (dsDNA), termed A-, B-, and C-forms [20–22]. While the B-form is the accepted canonical form of dsDNA under typical solution conditions, the C-form was first observed in Li salts of DNA fibers [21, 23] and was later reported more broadly in fibers under conditions of high salt and low humidity [24, 25]. The C-form of DNA has been considered a distorted version of the B-form with a twist per base pair ∼2–3° larger than the B-form [26, 27]. The C-form of DNA has recently been suggested to play a role in homologous recombination [28] and for certain sequences involved in strong bending [29].

In MD simulations, B- and C-form DNA can, in addition to the characterization by twist, be distinguished by the relative populations of two backbone conformations known as BI and BII, which reflect different torsional states in the DNA backbone. B-DNA is characterized by a predominance of the BI state, whereas an increased population of the BII conformation is associated with structural features observed in C-form DNA, including the higher helical twist [29, 30].

Work on DNA using circular dichroism (CD) spectroscopy has suggested changes of the DNA helix at very high salt concentrations, up to ∼10 M monovalent concentration [31, 32]. The observed changes in the CD spectra were attributed to the canonical B-form helix transitioning to the C-form in solution [31–34]. Similar to the MT-based twist measurements at lower salt, Li^+ was found to have the largest effect on the observed spectra of all monovalent ions investigated. However, the interpretation of the CD spectroscopy results has subsequently been challenged [35, 36] and has recently been revisited with additional measurements on circular DNA [37]. Taken together, the evidence for C-DNA in solution remains controversial, and it is an open question to what extent the high twist C-form conformations observed under low humidity in fiber diffraction data are indeed also populated in solution.

Simulations have also begun to address conformational shifts and B- to C-DNA transitions [29]. Several force fields including CHARMM36 [38] and the AMBER-based force fields OL21 [39], parmbsc1 [40], and TUMUC1 [30] improve DNA backbone accuracy by refining torsional parameters and enhancing the BI/BII equilibrium. However, the question of C-DNA formation under high salt conditions remains largely unexplored in MD simulations.

Here, we use single-molecule MT measurements (Fig. 1A) to systematically monitor changes in DNA for high alkali ion concentrations, Li^+ in particular, up to 8 M. The results suggest that DNA twist increases with increasing Na^+, K^+, Cs^+, and Li^+ concentrations up to 4–5 M, i.e. well beyond 1 M that was previously investigated. At even higher Li^+ or Cs^+ concentrations, the DNA twist saturates and even decreases again, which challenges the previous claims of C-DNA formation at high LiCl concentrations. Complementary measurements using CD spectroscopy reveal change in the spectra fully consistent with previous experiments and indicative of structural changes of the DNA helix even beyond 5 M LiCl. Our all-atom MD simulations in LiCl support the experimental findings and reproduce the observed twist trends, in particular when ion activity is considered. The simulations further indicate that B-form DNA remains stable under high salt, while C-form conformations are not maintained. Together, these approaches provide a comprehensive view of DNA behavior in high salt conditions and challenge longstanding assumptions about high-salt-induced structural transitions.

Materials and methods

Chemicals

For DNA incubation, 1× phosphate-buffered saline (PBS; 10 mM phosphate buffer, pH 7.4, 138 mM NaCl, 2.7 mM KCl; Sigma-Aldrich), prepared with ultrapure water (Milli-Q; Millipore), was used. Tris at 10 mM (pre-set, pH 7.0, pHast Pack; Sigma-Aldrich), prepared with ultrapure water (Milli-Q; Millipore), was used for salt solution preparation, unless stated otherwise. A 0.1–5 M concentration of NaCl (99.5%, p.a., ACS, ISO; Carl Roth), 0.1–4 M KCl (99.5%, p.a., ACS, ISO; Carl Roth), 0.1–12 M LiCl (99%, p.a., ACS; Carl Roth), and 0.1–7 M CsCl (99.999%, p.a., Ultra Quality; Carl Roth) were prepared using 10 mM Tris (pH 7.0) at room temperature (∼22°C) in a volumetric flask (25 ± 0.04 ml; DURAN) and stored in glass vials (Sigma-Aldrich). For CsCl, additional salt solutions were prepared both in 10 mM Tris–HCl pH 8.0 and in the absence of buffer. Salts were protected against humidity. KCl at 100 mM was used as the reference condition for MT measurements, matching our previous choice of reference condition [6]. Refractive indices were determined ($\lambda = 589.3$ nm, 21°C; Abbe Refractometer 3T, Atago) to confirm the salt concentration and for MT analysis (Supplementary Figs S1 and S2; Supplementary Table S1). Our results for the refractive indices are in excellent agreement with literature values [41] and expand the range previously covered for LiCl.

DNA construct and flow cell preparation

Our MT measurements used a 20.6 kbp DNA construct, based on the λ-phage DNA sequence, with a GC content of 46% and prepared as described previously [42, 43], unless stated otherwise. Control measurements used a 7.9 kbp DNA construct with 56% GC content that was employed previously for similar measurements [6, 44]. The DNA constructs are designed to allow torsionally constrained attachment to the bottom glass surface of a flow cell and superparamagnetic

beads, respectively. The sequences of our DNA constructs are representative of "random", genomic DNA and provide effectively a sequence averaged view of DNA's response, as is typical for MT measurements. In brief, PCR-generated DNA fragments (∼600 bp) labeled with multiple biotin or digoxigenin groups were ligated to the DNA (20.6 kbp or 7.9 kbp), to bind 1.0 μm diameter streptavidin-coated magnetic beads (Dynabeads MyOne Streptavidin C1, Thermo Fisher Scientific Baltics UAB, LT) and the flow cell surface, respectively. To attach the DNA to the flow cell, the bottom coverslip was first modified with (3-glycidoxypropyl)trimethoxysilane. Next, 100 μl of a 5000× diluted stock solution of polystyrene beads (Polysciences, USA) in ethanol (Carl Roth, Germany) was dropcasted on the silanized slides, and left to dry while covered. The polystyrene beads serve as fiducial markers for drift correction. A laser cutter was used to cut openings with a radius of 1 mm in the top coverslip for buffer exchange. The two coverslips were glued together by a single layer of melted Parafilm (Carl Roth, Germany), forming an ∼25 μl channel that connects the inlet and outlet opening of the flow cell. After flow cell assembly, 100 μg ml^{-1} anti-digoxigenin (Abcam plc, UK; Roche, Switzerland) in 1× PBS was introduced and incubated for at least 1 h. To reduce non-specific interactions of the DNA and beads with the flow cell surface, the flow cell was flushed with 100 μl of 50–250 mg ml^{-1} bovine serum albumin (Sigma-Aldrich, USA), incubated for 1 h, and rinsed with 600 μl of 1× PBS. Next, the DNA construct was attached to streptavidin-coated beads by incubating 2 μl of 0.2 ng μl^{-1} DNA stock solution and 2 μl of MyOne beads in 200 μl of 1× PBS (Sigma-Aldrich, USA) for 5 min, and subsequently introduced into the flow cell for 20 min to allow formation of digoxigenin–anti-digoxigenin bonds. Subsequently, the flow cell was rinsed with 2 ml of 1× PBS to flush out unbound beads.

Magnetic tweezers instrument

Multiplexed single-molecule MT experiments were performed as previously described [6, 45, 46]. For twist control and the application of precisely calibrated forces, we employ a pair of permanent magnets (5 × 5 × 5 mm^3, Supermagnete, Switzerland) arranged in vertical geometry [47] with a gap of 1 mm and mounted in a holder that is controlled by a translation motor (M-126.PD2, PI) and a rotation motor (C-150.PD, PI). The motors are controlled, and magnetic beads are tracked in real-time by processing the camera images using a custom-written LabView program [48, 49]. An LED (69 647; Lumitronix LED Technik GmbH) provides illumination. The field of view is imaged using a ×40 oil-immersion objective (UPLFLN ×40; Olympus), together with a CMOS sensor camera (12M Falcon2; Tele-dyne DALSA). A frame grabber (PCIe 1433; National Instruments) collects images recorded at 58 Hz. A look-up table is created by moving the objective with a piezo stage (PifocP726.1CD, PI). Position measurements were corrected for the change in refractive index with salt concentration (Supplementary Fig. S2). Force calibration was performed based on the transverse fluctuations of the 20.6 kbp DNA tethers using the equipartition theorem as described previously [50, 51]. The measurement uncertainty in the forces is 10% and dominated by bead-to-bead variations [47, 51, 52]. For this setup geometry, it has been shown previously that the forces (for a given bead) across the field of view vary by <3% [53].

Magnetic tweezers twist measurements

Suitable dsDNA tethers were identified by rotating the external magnets to introduce negative supercoiling under high tension ($F \geq 5$ pN), where for single DNA tethers the formation of plectonemes at negative linking differences is suppressed due to melting and the extension remains unchanged [54]. In contrast, if multiple tethers are attached to the same bead, negative supercoiling results in braiding, which decreases tether extension. To assess whether DNA tethers were torsionally constrained, positive linking differences are introduced at low force ($F = 0.5$ pN), which results in plectoneme formation and a corresponding decreasing DNA extension for torsionally constrained tethers. In nicked DNA tethers, no linking difference can be introduced, and the extension remains constant on magnet rotation. Beads bound by multiple tethers or nicked tethers are discarded from further analysis.

In principle, the position of attachment of the DNA to the bead can modify the observed extension response (and ensuing force–extension behavior) [55, 56]. However, the corresponding corrections are relatively minor for the combination of long DNA (∼7 μm contour length) and small beads (1 μm diameter) used here, and the resulting uncertainty would only give a constant offset that does not affect the response to applied turns. Therefore, attachment positions were not discriminated.

Following bead selection and testing, the buffer in the flow cell was exchanged for a buffer comprising 100 mM KCl and 10 mM Tris (pH = 7.0), since this is the reference condition employed previously [6]. We recorded extension–rotation curves by changing the magnet rotation, and thus the linking number ΔLk, in steps of five turns at low force ($F = 0.25$ pN, unless stated otherwise). At each step of five applied turns, the extension of the tether is recorded for 6–10 s (at a camera rate of 58 Hz), and the mean extension is calculated. Subsequently, the buffer was exchanged to vary salt conditions.

For CsCl solutions prepared using 10 mM Tris–HCl at pH 7, we occasionally observed surface interaction of the beads or collapse of the DNA molecule at CsCl concentrations ≥ 3 M. Therefore, to investigate the role of salt and buffer, we additionally performed measurements in the absence of buffer (i.e. using only CsCl in Milli-Q water) and in 10 mM Tris–HCl at pH 8. In addition, we performed measurements at forces of 0.25 pN and 0.5 pN for comparison.

To ensure equilibration, we flushed a large volume of buffer at each new concentration through the flow cell (>300 μl or ∼12 cell volumes). During buffer exchange, we apply high force $F = 2$ pN, to ensure that the tethered beads do not rotate under the liquid flow and maintain constant linking number.

Circular dichroism measurements

CD spectra were collected using a spectropolarimeter (J-810-150S, JASCO, Japan) equipped with a temperature controller (20°C; CDF-426S, JASCO, Japan) in 10 × 10 mm sealable quartz cells (Hellma Analytics). Samples were prepared using the same stock for buffer and salt solution used for MT measurements (see above), i.e. 12 M LiCl (LiCl; ≥ 99%, ACS; Carl Roth), but employed 40 μg ml^{-1} λ-DNA [0.3 μg μl^{-1}, 48.5 kbp, 10 mM Tris–HCl (pH 7.6) and 1 mM EDTA; catalogue number SD0011 from Thermo Scientific] with a final volume of 2500 μl. We employed λ-DNA, instead of the functionalized DNA construct used in MT measurements, since the functionalized DNA is difficult and wasteful to produce in

sufficient quantities for CD spectroscopy and since the labels used for attachment in the MT might interfere in the spectroscopic measurements. Measurements were performed with a scan rate of 20 nm min^{-1}, and spectra were obtained as the accumulation of three scans. The individual DNA concentrations were determined from the absorbance using a molar absorptivity at 260 nm of 6600 M^{-1} cm^{-1}. CD was expressed as $\Delta\epsilon = \epsilon_L - \epsilon_R$ in units of M^{-1} cm^{-1} (Supplementary Table S2). The molarity (M) was related to mean residual weight in the DNA samples, i.e. to the nucleotide concentration, which is independent of DNA length.

Molecular dynamics simulations

We performed all-atom MD simulations of a 33 bp dsDNA, in each case comparing simulations using the B- and the C-form as starting structures. If not stated otherwise, the Gromacs software package, version 2020.7 [57] was employed for system preparation and simulation. For electrostatics, the particle-mesh Ewald (PME) summation was used with an order of 4 and a Fourier space grid of 0.12 nm. Furthermore, a cut-off of 1.2 nm was employed for Lennard–Jones and close Coulomb real space interactions. A time step of 2 fs was used and the LINCS algorithm was employed to constrain hydrogen bonds.

To generate structural models, we used the DNA sequence 3′-GAGAT-GCTAA-CCCTG-ATCGC-TGATT-CCTTG-GAC-5′, the same as used previously [6], and employed Web 3DNA 2.0 [58] to generate starting structures based on fiber models in B- and C-form DNA geometry, respectively (ID 4 and 7 in the nomenclature of [26]). The resulting B-form structure was in close agreement with our previous model, with a root mean square displacement (RMSD) of 1.0 Å for the backbone atoms, whereas the RMSD between the models for B- and C-form DNA was 4.1 Å. One prominent difference between the two generated structures is the average helical twist, which is 38.7° bp^{-1} for the C-form, compared with 36.1° bp^{-1} for the B-form. In our simulations, we tested several DNA force fields in combination with specific ion and water models. As one combination, which was also employed in previous work [6], we used the parmbsc1 force field [40] for DNA, combined with Mamatkulov–Schwierz ion parameters [59], and TIP3P water [60], across a broad range of ion concentrations. The choice of the ion force fields was motivated by the fact that the parameters were optimized to yield accurate ion–water and ion–ion interactions as judged by the comparison with experimental solvation free energies and activity coefficients up to 3 M salt concentration [59]. For the larger salt concentrations, we computed the radial distribution functions, determined the activity derivatives from Kirkwood–Buff theory [61, 62], and compared them with experimental data (Supplementary Methods). Even at the highest salt concentration, there was no indication of clustering or crystal formation. The same choice of force fields was also employed for simulations with NaCl at 1.0 and 4.4 M concentrations, discussed in the Supplementary Methods.

To set the ion concentration in the simulations, we initialized simulations at defined molalities (i.e. moles of ions per kg of water). Comparison with the experimental data, however, required concentration in molarity (i.e. moles of ions per liter of total volume). Therefore, we calculated the box volumes, by averaging the volume over the time of the production simulations in the NPT ensemble. In Supplementary Tables S3 and S4, we report the concentrations in molality and in molarity, and the volumes for the parmbsc1 simulations used in this work. Throughout the work, we report the concentrations in molarity, since this is what is controlled experimentally, unless otherwise noted.

We carried out simulations using the CHARMM36 force field [38] for DNA, while maintaining the same ion and water parameters, for eight LiCl concentrations from 1 to 6.5 M (1 m to 8 m on the molality scale). Further, we tested the OL21 force field [39] for DNA, again with the same ion and water models, at two LiCl concentrations: 1 M and 4.4 M (1 m and 5 m on the molality scale). Similarly, simulations using the TUMUC1 force field [30] were performed at 1 M and 4.4 M LiCl with identical ion and water settings. Finally, to reproduce the conditions used by Strelnikov *et al.* [29], we conducted simulations using parmbsc1 for DNA, Joung–Cheatham ion parameters [63], and TIP4P-Ew water [64], at 1 M and 4.5 M LiCl. To further assess the influence of the water model, we performed simulations with OPC water together with parmbsc1 for DNA and Mamatkulov–Schwierz ion parameters at three LiCl concentrations: 1.0, 4.4, and 7.8 M (Supplementary Methods).

For all systems, the dsDNA structures in B- or C-form were put in a rhombic dodecahedron box with a minimal distance of 1.5 nm to the edges and filled with water molecules. The initial simulation protocol consisted of energy minimization followed by NVT and NPT simulations. During this protocol, the heavy atoms of the nucleic acids were restrained [1000 kJ $(mol\ nm^2)^{-1}$]) to allow solvent equilibration. Energy minimization with the steepest descent algorithm used a maximum of 50 000 steps. Subsequently, we used NVT and NPT simulations of 1 ns each for obtaining systems at ambient conditions. In these simulations, the temperature of 300 K was maintained using the velocity rescaling thermostat [65] with a coupling constant of 0.1 ps. In the NPT simulations, the isotropic Parrinello–Rahman barostat [66] with a coupling constant of 5 ps was additionally employed.

After this initial protocol, we first performed 300 ns simulations in the NPT ensemble without restraints. Starting from the final equilibrated structures, three 300 ns production runs were carried out, and the first 100 ns of each trajectory were discarded from the analyses. The simulation volumes determined from NPT ensemble simulations (Supplementary Tables S3 and S4) fluctuate by <0.2% (or $\leq$3 nm^3) in the course of the trajectories. The reported volumes include the volume of the DNA, which is 2% (~40 nm^3) of the total simulation volume. For the setup with the highest LiCl concentration employing the parmbsc1 force field and TIP3P water, we extended the simulations up to 1.2 μs. There are no significant differences for the twist for longer time intervals and we conclude that the 600 ns after equilibration are sufficient to obtain converged results (Supplementary Methods).

The helical properties were determined with the 3DNA software [26, 67] by using the do_x3dna software package together with its dnaMD python module [68] and in-house scripts. In these analyses, we leave out the first and the last three base pairs unless otherwise noted. Omitting more base pairs from the analysis does not change the resulting twist significantly (Supplementary Methods) for DNA chains longer than 15 bp, in agreement with previous observations [6]. To determine the number of adsorbed ions, we counted for each frame all Li^+ ions that were within a cut-off distance of 0.3 nm to any non-bridging backbone oxygen atom of the dsDNA

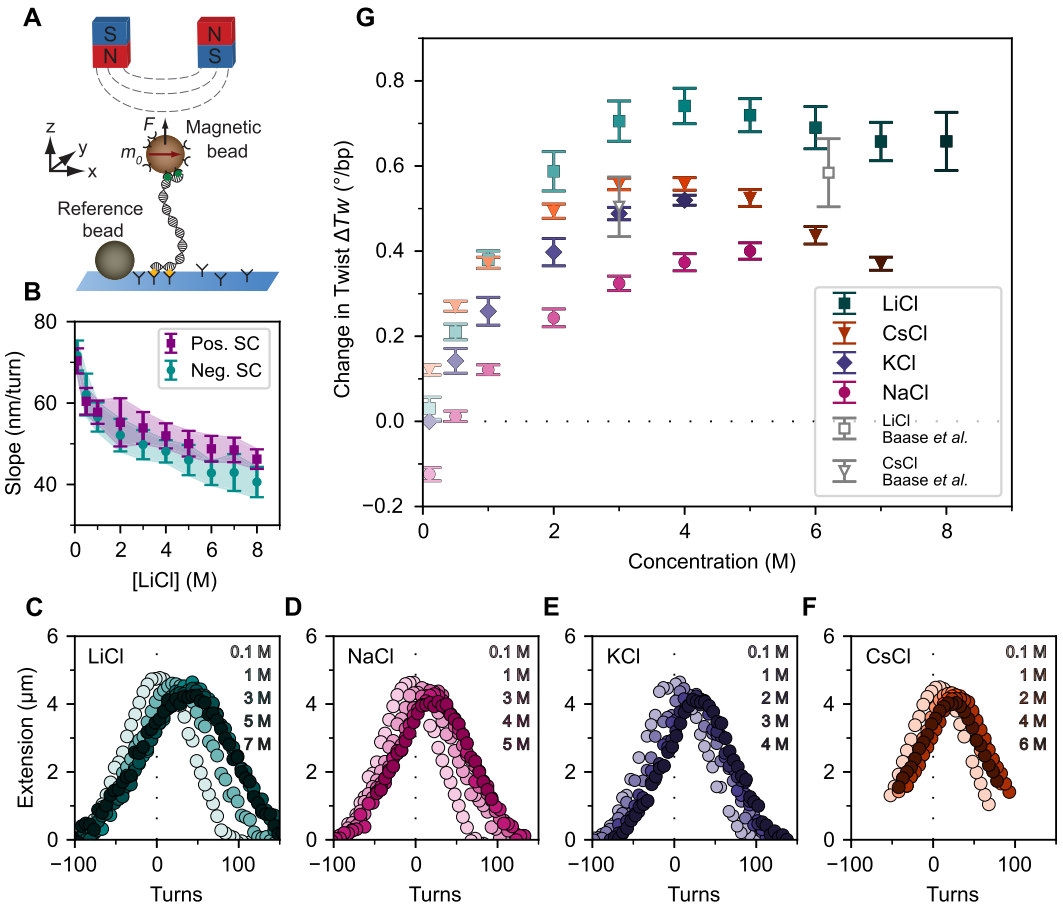

Figure 1. Magnetic tweezers probe changes in DNA twist with increasing monovalent salt concentration. (**A**) Schematic of the magnetic tweezers setup. A DNA molecule is tethered between the flow cell surface and a magnetic bead via multiple attachment points at both ends. External magnets enable applications of forces and torques to the DNA tether. Reference beads are tracked for drift correction. (**B**) Slopes of extension versus turns in the plectonemic regime from fits to the rotation curve data [including the data in (C)] at $F = 0.25$ pN as a function of LiCl concentration for positive (purple squares) and negative (cyan circles) plectonemic supercoils. Data points and error bars are the mean ± SD from at least 11 molecules. Similar data for other ions are shown in Supplementary Fig. S9. DNA extension versus applied rotation measurement in the presence of increasing concentrations of (**C**) LiCl, (**D**) NaCl, (**E**) KCl, and (**F**) CsCl. Zero turns is defined as the center of the extension versus rotation curves in 100 mM KCl, i.e. the linking number at which the DNA is torsionally relaxed in the reference condition of 100 mM KCl. The curves shift systematically to larger turns with increasing salt concentration, indicative of increasing helical twist with increasing concentration. Data are at $F = 0.25$ pN. (**G**) Change in DNA twist determined from the centers of the rotation curves [including the data in (C–F); Supplementary Fig. S3] as a function of monovalent salt concentration. Data are relative to 100 mM KCl and represent the mean ± SD from at least three and typically 10–20 molecules. The gray data points were obtained by analytical ultracentrifugation and are taken from Baase and Johnson [35].

and averaged this over each trajectory. For each concentration and DNA form, averages and standard errors of the mean (SEMs) were estimated from the three independent production runs. Values reported in our previous study [6] were employed for determining changes of helical properties relative to 0.10 M KCl and for the results up to a maximum concentration of 1 M.

For obtaining representative structures, we employed clustering with the algorithm of Daura *et al.* [69]. Structures were taken from all three production runs per concentration and initial B- or C-form. A cut-off of 0.5 nm was employed to group similar conformations based on RMSD. In each case, the largest cluster encompassed at least 90% of all structures and the central structure of this cluster is therefore considered to be representative.

Gromaps [70] was used to analyze the three-dimensional cation distribution, and the results were visualized with pymol (The PyMOL Molecular Graphics System, Version 3.1 Schrödinger, LLC, NY, USA).

Results

Single-molecule magnetic tweezers measurements determine DNA twist for high salt concentrations

We used single-molecule MT to manipulate 20.6 kbp DNA molecules tethered between a functionalized flow cell surface and small, 1.0 µm diameter, superparamagnetic beads (Fig. 1A; see the Materials and methods). The MT allow the application of precisely calibrated stretching forces and control of the rotation of the magnetic bead, and thus the linking number of the tethered molecules [47, 71–74]. We systematically measured the DNA tether extension as a function of applied turns under a low stretching force (Fig. 1C–F). In this low force regime, the force response of DNA is dominated by entropic stretching and well described by the inextensible worm-like chain model [75, 76]. The response of the tether extension to applied turns is approximately symmetric for over- and underwinding of the helix, and the DNA undergoes a buckling transition for both positive and negative applied turns

Table 1. Change in DNA twist (relative to 100 mM KCl) induced by alkali ions

Concentration (M)	LiCl ΔTw (° bp^{-1})	NaCl ΔTw (° bp^{-1})	KCl ΔTw (° bp^{-1})	CsCl ΔTw (° bp^{-1})
0.1	0.03 ± 0.03	−0.12 ± 0.02	0	0.12 ± 0.01
0.5	0.21 ± 0.02	0.01 ± 0.01	0.14 ± 0.03	0.27 ± 0.01
1	0.38 ± 0.02	0.12 ± 0.01	0.26 ± 0.03	0.37 ± 0.01
2	0.59 ± 0.05	0.24 ± 0.02	0.40 ± 0.03	0.49 ± 0.02
3	0.71 ± 0.05	0.32 ± 0.02	0.49 ± 0.02	0.56 ± 0.01
4	0.74 ± 0.04	0.37 ± 0.02	0.52 ± 0.01	0.56 ± 0.01
5	0.72 ± 0.04	0.40 ± 0.02		0.52 ± 0.02
6	0.69 ± 0.05			0.44 ± 0.02
7	0.66 ± 0.05			0.37 ± 0.02
8	0.66 ± 0.07			

Data are the mean ± SD from at least three, and typically 10–20, measurements.

[71, 77]. Past the buckling transition, the DNA forms positive or negative plectonemic supercoils, respectively, marked by a linear decrease of the tether extension with the number of applied turns (Fig. 1B–F; Supplementary Fig. S3). The rotation–extension curves reveal systematic shifts to positive turns with increasing ion concentration (Fig. 1). We quantify the shifts by fitting the linear slopes in the plectonemic regime and determining the intersection points of the slope at positive and negative turns [6, 78] (Supplementary Fig. S3). Importantly, the changes are fully reversible: if the salt concentration is lowered again, the curves return to their previous position (Supplementary Fig. S4).

To facilitate direct comparison with previous measurements [6], we used 100 mM KCl as our reference condition. This choice of reference condition was motivated by the considerations that (i) 100 mM monovalent ions correspond, approximately, to physiological ionic strength and intracellularly K^+ is the most abundant cation, (ii) 100 mM KCl is a condition that was included in previous studies of the salt dependence of DNA twist [4, 5], and (iii) 100 mM KCl is readily and robustly accessible both in MT experiments and in MD simulations.

DNA twist increases up to 4–5 M monovalent ion concentration

We find that DNA twist increases with increasing LiCl, NaCl, KCl, and CsCl concentration, consistent with previous measurements (Fig. 1G). When comparing our data (obtained with a 20.6 kbp DNA with 46% GC content) with previous MT measurements using a different DNA construct (7.9 kbp with 56% GC) across monovalent ions, we find slightly different but overall similar changes in twist compared with 100 mM KCl (Supplementary Fig. S5). The data suggest that the changes in DNA twist with salt concentrations are relatively independent of DNA sequence, similar to what was observed by Zhang *et al.* [8] up to 1 M monovalent salt concentration. However, the data also reveal small differences, implying that the effect on DNA twist of different salts might depend on details of the DNA used. We carried out additional measurements with the 7.9 kbp DNA construct for LiCl and find a slightly larger twist for LiCl relative to 100 mM KCl for the 56% GC construct compared with the 46% GC construct (Supplementary Fig. S6), but no differences in overall trend. Interestingly, we observe a significant increase of DNA twist when increasing ion concentration beyond 1 M. For all tested ions, LiCl, NaCl, KCl, and CsCl, the twist increases steadily up to 3–4 M. For NaCl and KCl, we continued measurements until the maximum aqueous solubility (4 M for KCl and 5 M for NaCl), reaching a change in twist of 0.4 and 0.5° bp^{-1}, respectively (Fig. 1G), relative to the reference conditions of 100 mM KCl.

LiCl induces the largest DNA twist of all the ions tested. Similar to the other ions, the twist increases for LiCl concentrations beyond 1 M: from ∼0.4° bp^{-1} at 1 M to ∼0.74° bp^{-1} at 4 M, all again with respect to the 100 mM KCl condition (Fig. 1G; Table 1; Supplementary Fig. S7). Beyond 4 M LiCl, the rotation–extension curves do not shift further along the turns axis, suggesting that the average twist of the DNA helix remains approximately constant and even slightly decreases (though values remain within experimental error) upon further increasing the concentration (Fig. 1G). Measurements with the higher GC content, 7.9 kbp DNA construct found slightly higher values of DNA twist at 3–5 M LiCl, up to ∼0.9° bp^{-1}, but exhibit identical trends to those observed for the 20.6 kbp DNA, with an increase in twist up to 5 M LiCl, and eventual saturation and decrease of the twist at even higher concentrations (Supplementary Fig. S6). For LiCl, concentrations >8 M resulted in detachment of the DNA constructs in the flow cell, preventing measurements up to the solubility limit of LiCl (∼14 M).

CsCl has a high solubility in water, up to 7–7.5 M [41], enabling measurements over a large ionic range. Consistent with previous observations [6], we find that at low concentrations (100 mM), CsCl induces the largest twist of all monovalent ions tested, even larger than LiCl. The twist induced by CsCl is surpassed by LiCl at intermediate concentrations but continues to exceed both NaCl and KCl. At high concentrations (>2 M), the twist induced by CsCl initially continues to increase up to 0.6° bp^{-1} at 3–4 M. Similar to the trend observed for LiCl, the twist subsequently decreases at even higher concentrations. The decrease in twist at the highest concentrations is more pronounced for CsCl than for LiCl, and at 7 M CsCl the observed change in twist is reduced to values found for ∼1 M CsCl.

We occasionally observed beads sticking to the surface and collapse of the DNA molecules at high concentrations of CsCl (Supplementary Fig. S8; see also the Materials and methods). Therefore, we carried out additional measurements with different buffers and at different forces, and found that an elevated pH of 8 and consequently an increased buffering capacity appears to stabilize DNA behavior. Importantly, after excluding traces suffering from either beads or DNA getting stuck, we find fully consistent values for the change in DNA twist with CsCl concentrations, independent of applied force or buffer used (Supplementary Fig. S9). We compare our MT data for the change in twist induced at high salt concentrations with previous results obtained by ultracentrifugation for 6.2 M LiCl and 3.0 M CsCl reported by Baase *et al.* (Fig. 1G,

gray symbols) [35] and we find that the results from the two different methodologies are in good agreement, within experimental error.

Overall, the changes in twist are well described by a square root dependence up to 2 M for all salts studied, in good agreement with previous measurements (Supplementary Fig. S10) and with the predictions based on classical electrostatic screening reducing the repulsive interactions of the charged DNA backbone [6]. However, for concentrations ≥ 4 M, we observe clear deviations from this model, and the observed changes in twist clearly fall below the predictions of the square root dependence (Supplementary Fig. S10). For both LiCl and CsCl, we observe changes in the trend for DNA twist similar to changes in force stability and melting temperature previously attributed to DNA charge inversion by Zhang *et al.* [2] and Wei *et al.* [79]. For KCl, we did not observe a trend inversion, probably because of its limited solubility. Similarly, the smaller trend deviation observed for NaCl might be due to a smaller inversion of DNA charge, as observed recently for single-stranded DNA (ssDNA) [79]. We note that for all tested conditions, the increase in twist compared with approximately physiological conditions is $\leq 0.9^\circ$ bp^{-1}, which is well below the twist suggested for C-form DNA.

Changes of the slope in the plectonemic regime

The DNA tether extension decreases linearly with increasing (absolute) linking number in the plectonemic regime, and the slope in this regime provides a measure for the size of the plectonemes [80, 81]. We observe changes in the slope of the decrease in extension with applied turns (Fig. 1B; Supplementary Fig. 11), in good agreement with previous measurements with MT [82, 83]. At low salt concentrations (≤ 3 M), the slopes are equal in magnitude for positive and negative plectonemes for all salts investigated (Fig. 1B; Supplementary Fig. S11). Interestingly, at higher salt concentrations, the observed slopes remain mostly within experimental error but tend to be larger for positive than for negative supercoils, indicating possible—overall small—changes in helix or plectoneme geometry. We note that these changes are unlikely to be due to (partial) denaturation of the helix, since the curves were recorded at very low forces ($F = 0.25$ pN), where torque-induced melting is unlikely to occur, in particular since the pH of the solution remains close to neutral (Supplementary Fig. S12).

Circular dichroism spectra suggest changes in DNA conformation at high salt concentrations

To further study the changes in DNA induced by high salt concentrations and in particular to compare these with previous reports [31, 32, 34, 37], we measured CD spectra. For 100 mM monovalent ion concentrations, the CD spectra present three bands above 210 nm, with positive bands around 225 nm and 280 nm and a negative peak around 250 nm (Fig. 2A; Supplementary Fig. S13), in line with the well-established CD spectra of canonical B-form DNA [84]. At 100 mM salt concentration, the band at 280 nm exhibits some dependence on ion identity (Supplementary Fig. S13), in line with previous observations [34].

In the presence of high concentrations of LiCl (1–8 M), the band around 280 nm is systematically reduced and a sign change occurs above 4 M LiCl. The effect of salt on this spectral region of DNA has been widely reported, and

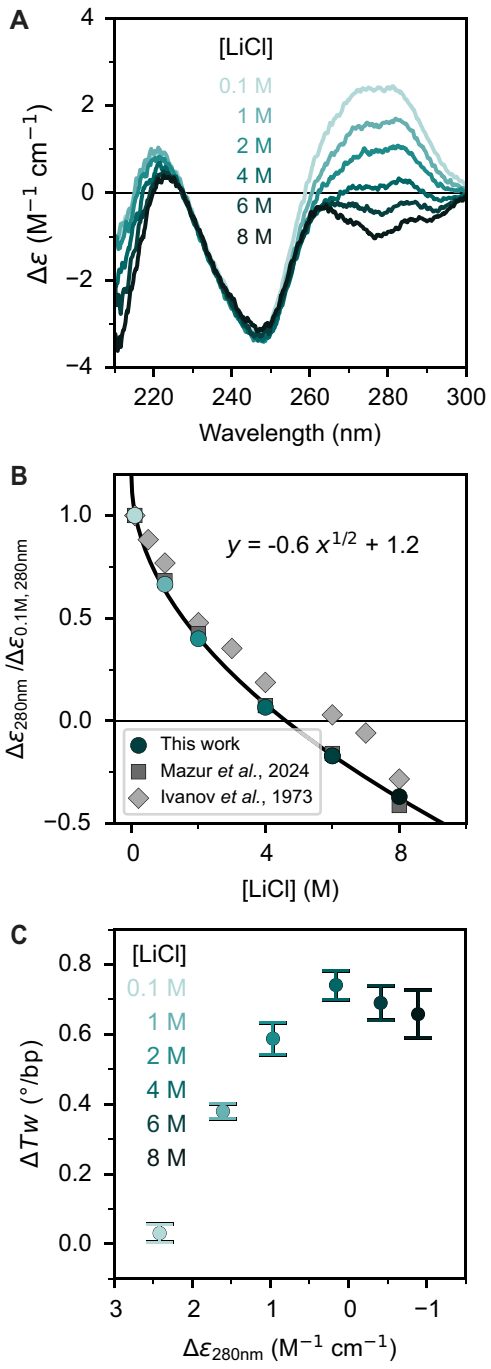

Figure 2. Effect of increasing LiCl concentration on CD spectra of DNA. (**A**) CD spectra of DNA (λ-DNA, 40 μg ml^{-1}) for increasing LiCl concentrations (from light to dark teal). Spectral changes are observed around the 280 nm band as the LiCl concentration is increased. Spectra are an accumulation of three scans and normalized to the nucleotide concentration. (**B**) Differences in the molar absorption at 280 nm for increasing LiCl concentrations. Data are normalized to the 100 mM LiCl condition. The solid line is a fit of a square root concentration dependence. Circles are the relative intensity at 280 nm in the spectra in (A). Squares and diamonds are data taken from [37] and [34], respectively. (**C**) Comparison of the change in DNA twist (Fig. 1G) and the difference in the molar absorption at 280 nm [from (A) and (B)] for increasing LiCl concentrations. For additional data, see Supplementary Fig. S11. Symbols are the ΔTw (mean ± SD from at least 11 molecules) compared with the difference in molar absorption values at 280 nm from the spectra in (A).

our experimental results are in good agreement with the observed changes in CD in previous work, using different DNA constructs with different sequences [31, 32, 34, 37] (Fig. 2B). Control measurements at different DNA concentrations show no significant dependence on DNA concentration (Supplementary Fig. S13), suggesting that intermolecular interactions, finite concentration effects, or aggregation are unlikely to play an important role in the changes in the CD spectra for the linear DNA used in our study. The change in the CD band at 280 nm follows a power law and scales with the square root of the salt concentrations over the entire investigated salt range, in excellent agreement with the observed changes in CD in recent work on linearized plasmids [37] (Fig. 2B; Supplementary Table S2).

To characterize the changes in DNA structure revealed by CD spectroscopy, we analyzed the data by singular value decomposition (SVD) (see Supplementary Fig. S14 for details). We find that the CD spectra are well described by two components with large singular values, with a third somewhat marginal signal-containing component. Unlike protein or RNA folding [85–87], the weights of our basis functions show a gradual evolution, lacking a clear sigmoidal transition. Interestingly, the coefficient associated with the second basis function displays a power law dependence similar to the CD intensities observed at 280 nm. Overall, the SVD analysis indicates gradual changes in the CD spectra and not the presence of two characteristic spectra or states.

The trend in the CD spectra, in particular at 280 nm, is similar to the scaling of DNA twist observed for alkali salts up to 1 M [6], but unlike the behavior of DNA twist as determined by MT measurements at high salt concentrations (Fig. 1). From the MT measurements, we find the maximum change in twist for all four salts studied, LiCl, NaCl, KCl, and CsCl, to be at 4–5 M (Fig. 1G; Table 1). For LiCl, we directly compare the change in twist with the change in CD at 280 nm (Fig. 2C). Below 4 M, a similar trend in both $\Delta\epsilon_{280nm}$ and ΔTw is observed, as for other salts when data from previous work are compared (Supplementary Fig. S15), suggesting a correlation between helical twist and CD intensity at 280 nm. However, above 4 M, the decrease in $\Delta\epsilon_{280nm}$ is no longer paired with an increase in DNA twist, as it remains at $\sim 0.7^\circ$ bp^{-1} for LiCl. Together, these observations suggest that further changes in the CD spectra, including the sign change, beyond 4 M are not associated with a continued increase in overall DNA twist and result from different types of molecular changes.

MD simulations predict the change in DNA twist for high LiCl concentrations in qualitative agreement with experiments

We performed unbiased all-atom MD simulations using a 33 bp DNA duplex in solution with increasing LiCl concentrations up to 7.8 M (10 m on the molality scale). The DNA constructs used in the MD simulations are necessarily much shorter than the DNA used for MT measurements, since all-atom MD simulations with explicit water and ions of $\geq$ kbp DNA are currently beyond the scope of computational capabilities. However, previous work has shown that DNA twist can be reliably determined from simulations of DNA oligomers as used here and systematically compared with MT measurements on much longer DNA or RNA constructs [6, 78, 88, 89]. In addition, DNA conformations can be strongly

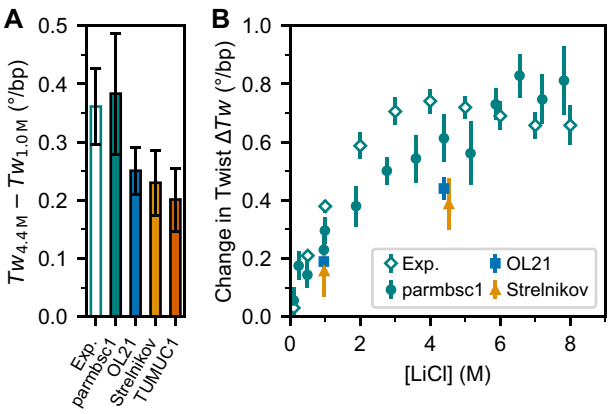

Figure 3. Change in DNA twist from MD simulations for different force fields as a function of LiCl concentration. (**A**) Increase in twist between 1.0 and 4.4 M LiCl from simulations with different force fields: parmbsc1 [40], OL21 [39], parmbsc1 with Strelnikov solvent representation [29], and TUMUC1 [30]. The experimental data value is for 4 M LiCl. (**B**) Change in twist as a function of LiCl concentration relative to 100 mM KCl from experiments and simulations with selected force fields. Experimental data points are from Fig. 1G and data points from simulations correspond to the mean ± SEM from six independent simulation runs.

influenced by sequence [90–92]. In our previous work [6], we demonstrated that sequence-dependent effects are evident in oligonucleotides up to 15 bp in length, but these effects average out in longer constructs, such as the 33 bp duplex analyzed here (see also below).

We focused on Li^+ as cation, as it shows the largest DNA twist in the experiments. We compared several DNA force fields (parmbsc1, OL21, TUMUC1, and CHARMM36) and the solvent representation by Strelnikov *et al.* for which B- to C-form transitions were observed for poly(AC) sequences [29]. In addition, we performed simulations with Na^+ with the parmbsc1 force field for 1.0 and 4.4 M concentrations (Supplementary Methods).

The predicted change in DNA twist induced by high LiCl concentrations relative to 0.10 M KCl varies markedly across different force fields (Supplementary Fig. S16). Notably, TUMUC1 and CHARMM36 predict a decrease in twist relative to 0.10 M KCl, contrary to experimental observations. Still, all force fields, except CHARMM36, capture the experimentally observed increase in twist with rising LiCl concentration relative to 1 M LiCl (Fig. 3A). The deviations from experiments with CHARMM36 are linked to frequent openings of the terminal base pairs observed for all salt concentrations (Supplementary Fig. S17). For TUMUC1, the discrepancy arises from excessive Li^+ binding to phosphate oxygens and nucleobase donor atoms (Supplementary Fig. S17). The deviations with TUMUC1 are not inherent shortcomings of the force fields themselves but reflect an unfavorable combination of DNA and ion force fields. Still, neither DNA force field is recommended for simulations of DNA in high salt conditions. The OPC water model is increasingly used in nucleic acid simulations due to its improved description of water electrostatics and related physical properties compared with TIP3P. We therefore assessed the influence of the water model on the predicted change in DNA twist using the parmbsc1 parameterization and replacing TIP3P with the four-site OPC model. While OPC correctly reproduces an increase in DNA twist with increasing LiCl concentration, the magnitude of the

effect is underestimated relative to both TIP3P-based simulations and experimental observations (Supplementary Methods; Supplementary Fig. S18).

Among the tested force fields, parmbsc1 combined with Mamatkulov–Schwierz ion parameters and TIP3P water shows the best agreement with experimental data (Fig. 3A, B; Supplementary Figs S16 and S18) and is therefore used for the subsequent analysis. It correctly reproduces both the sign and approximate magnitude of twist increase up to ∼0.8° bp^{-1} compared with 0.10 M KCl and provides qualitative agreement with the observed concentration dependence. The agreement between simulations and experiments improves further when differences in ion activities are accounted for by using activity derivatives; see below. Extending the simulations to 1.2 μs revealed no significant changes in DNA twist, and additional tests showed that the predicted twist changes are independent of DNA length (15–33 bp) at high salt concentrations, consistent with previous results at lower salt concentrations [5] (Supplementary Figs S19 and S20).

C-form DNA is unstable in high LiCl concentrations and rapidly converges to B-form in MD simulations

We initiated half of our simulations in an ideal B-form (low twist) and the other half in the C-form (high twist). In all cases, i.e. for all force fields and solvent representations, the C-form is not stable, and the twist decreases rapidly to the lower values characteristic of B-form DNA in the course of the simulations. Specifically, after equilibration, the twist is at least ∼2.5° bp^{-1} lower compared to the ideal C-form structure, independent of starting configuration. Even at the highest 7.8 M concentration (parmbsc1/Mamatkulov–Schwierz), the twist for the C-form quickly decayed within a few nanoseconds to a value typical for B-DNA (Fig. 4A). We note that a conversion from C- to B-form within the first few nanoseconds of the simulations is similarly observed for simulation with LiCl and the OPC water model and for simulations using 1 and 4.4 M NaCl (Supplementary Figs S21 and S22).

BI/BII populations provide an alternative means to distinguish between B- and C-form DNA, as the C-form of DNA has been experimentally associated with elevated BII populations at high salt concentrations [29, 93]. To further confirm that C-DNA does not form in our simulations, we analyzed these populations in detail for the parmbsc1/Mamatkulov–Schwierz simulations with TIP3P water and LiCl. The distributions of the ϵ–ζ dihedral angle difference, where negative values indicate BI and positive values BII populations, are nearly identical at 1 M and 7.8 M LiCl, with no systematic shift toward BII at higher concentrations (Fig. 4B). Consistently, the BII population remains within 21–23% across all conditions as is typical for B-DNA and far below the >40% expected for C-DNA [29].

In addition, we clustered structures from simulations at 7.8 M LiCl that started in C-DNA and compared the central structure with idealized B- and C-forms (Fig. 4C). The central structure of the largest cluster (90% of all structures) aligns more closely with the ideal B-form (RMSD 2.8 Å) than with the C-form (RMSD 5.5 Å), further supporting the absence of C-DNA in the simulations. In summary, twist, BI/BII populations, and structural alignment show consistently that C-form DNA is not stable in the simulations for different force fields, even at LiCl concentrations up to 7.8 M, and rapidly converges to the B-form.

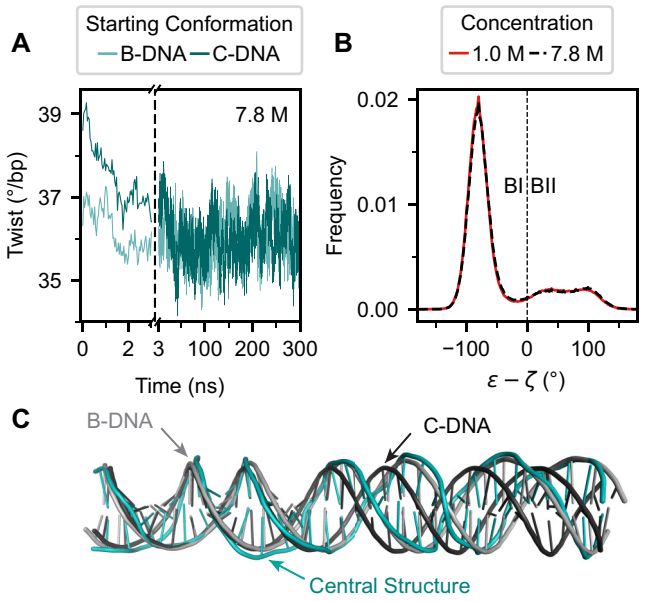

Figure 4. C-DNA is unstable in high LiCl concentrations and converges to B-DNA in MD simulations. (**A**) Time series of twist in 7.8 M LiCl initiated from an ideal B- and C-DNA structure. The twist for the C-form quickly decays to the value of B-DNA. (**B**) Histograms of the dihedral angles difference ϵ–ζ for 1 M and 7.8 M concentrations. The dashed vertical line indicates the separation between BI (ϵ–ζ < 0°) and BII (ϵ–ζ ≥ 0°) populations. (**C**) Central structure of the dominant cluster (90% of structures) from 7.8 M concentration simulations (teal) superimposed with ideal models of B- (light gray) and C-form DNA (black). The structures were aligned using the first 10 bp on the left. All simulations were performed with parmbsc1/Mamatkulov–Schwierz force fields.

MD simulations reproduce the experimental change in DNA twist as a function of the activity derivative

The change in twist obtained from simulations as a function of salt concentration shows two notable deviations from the experimentally determined values. First, the initial increase in twist in the simulations is less steep compared with experimental results (Fig. 3B). Second, while the experimental values saturate between 4 and 5 M salt concentration, the twist from simulations continues to increase and saturates at ∼6.5 M. The observed discrepancies suggest that while MD simulations can capture the sign and magnitude of DNA twist changes with high LiCl concentrations, they fail to describe the concentration dependence quantitatively. We next tested whether deviations between ion activities from simulations and experiments can explain the apparent deviations in concentration dependence.

Activity coefficients and their derivative provide direct insight into ion–ion and ion–water interactions [59, 94]. In simulations, activity derivatives can be directly accessed via Kirkwood–Buff theory [61, 62], and we used this approach to compare the activity derivatives from our simulations with experimental data (Supplementary Methods; Supplementary Figs S23 and S24). The comparison between the experimental and calculated activity derivatives as a function of the salt concentration (Fig. 5A) shows that the activity derivatives in the simulations are too low for concentrations >2.5 M. An underestimation of the activity derivative indicates that ion pairing between Li^+ and Cl^- is overestimated in the simulations [18, 59].

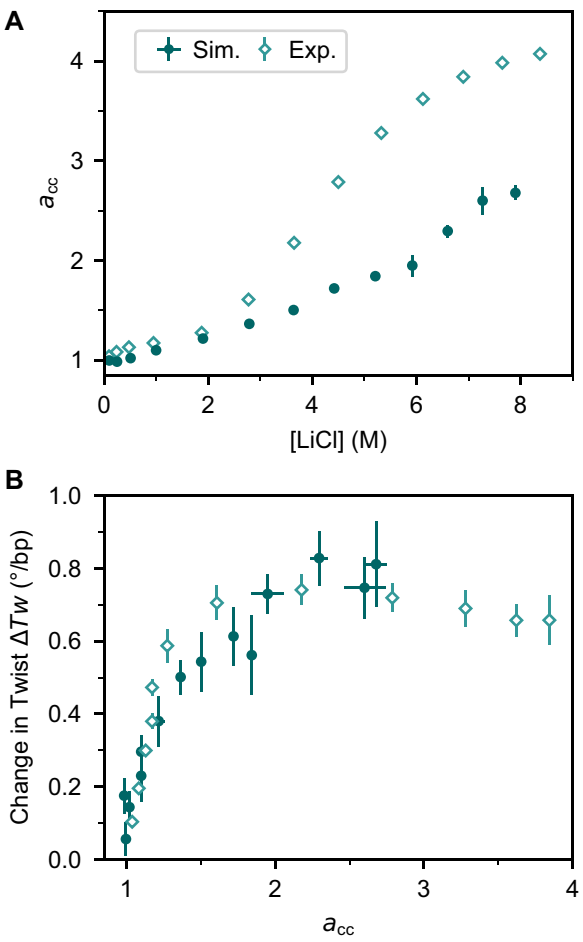

Figure 5. Change in twist as a function of the activity derivative. (**A**) Activity derivative a_{cc}as a function of the LiCl concentration from experiments [110] and current simulations using Kirkwood–Buff theory (Supplementary Methods). (**B**) Change in twist as a function of the activity derivative a_{cc} obtained from the a_{cc}–concentration relationship shown in (A) from experiments and simulations with parmbsc1 combined with Mamatkulov–Schwierz ion force field, and the TIP3P water model. Simulation points and error bars for a_{cc} indicate the mean and SEM from three independent simulations.

To account for the deviations between experiments and MD observed for LiCl, we compare experiments and simulations under conditions where anion–cation interactions are matched, using activity derivatives as the basis for comparison. Using activity derivatives instead of concentrations, we find significant improvement and quantitative agreement between experiments and simulations (Fig. 5B). Notably, the simulations capture the experimentally observed non-linear increase of twist including the steep increase at low activity derivatives, the slowing of twist change in the intermediate range, and the saturation at activity derivatives >2 (corresponding to an experimental concentration of ∼4 M).

Additional NaCl simulations similarly show a clear discrepancy between simulated and measured activity derivatives, again in particular at concentrations ≥ 2.5 M (Supplementary Fig. S25). This discrepancy very probably also explains why the NaCl significantly underpredicts the increase in DNA twist induced by high concentrations of NaCl (Supplementary Fig. S25).

We conclude that accurate predictions of DNA twist at high salt concentrations require proper treatment of both ion–ion and ion–water interactions as well as ion binding, while an imbalance leads to deviations between simulations and experiments. We find that comparing DNA properties as a function of activity derivative rather than concentration provides a more reliable and accurate approach. The observed deviations suggest, further, that refining the Li^+–Cl^- interactions (and similarly Na^+–Cl^- interactions) beyond standard combination rules at high salt concentrations, analogous to previous efforts under low salt conditions [94–96], is likely to represent an important next step for accurate high-salt MD simulations.

Mechanistic model for DNA twist in the high salt regime

To provide molecular insight into the non-linear increase and saturation of DNA twist with increasing activity derivative, we analyzed characteristic structural properties of DNA (Fig. 6). Overall, we find that changes in twist correlate strongly with the DNA radius, sugar pucker angle, and helical rise (Supplementary Table S5), consistent with previous findings in the low salt regime [6, 7]. The trends observed at low salt concentrations persist into the high salt regime: as salt concentration increases, more Li^+ ions adsorb to the DNA backbone, leading to enhanced electrostatic screening. This screening reduces phosphate–phosphate repulsion and results in a decrease in DNA radius (Fig. 6A). The narrowing of the helix is compensated by an increase in the sugar pucker angle (Fig. 6B) and a decrease in helical rise (Fig. 6C). Notably, the changes in twist with increasing activity derivative are non-linear: the initial sharp increase is followed by a slowing and eventual saturation at very high concentrations, for activity derivative ≥ 2, corresponding to ∼4 M salt (Fig. 5B). The same trend is also observed in the changes in radius and sugar pucker angle (Fig. 6A, B).

The underlying mechanism is closely linked to the number of specifically adsorbed Li^+ ions (Fig. 6D–G; Supplementary Fig. S26). In the low salt regime, the number of adsorbed cations increases rapidly, approaching full compensation of the negative DNA charge near activity derivative $a_{cc} = 1$ (corresponding to ∼1 M) with one Li^+ per phosphate group (dashed line in Fig. 6D). Beyond this point, charge reversal occurs, and the local effective DNA charge becomes positive, indicating overcharging consistent with previous observations for other monovalent cation–DNA interactions [2]. Overall, ion binding slows as the system approaches a stoichiometry of two Li^+ ions per phosphate group. Here, on average, two Li^+ ions are bound per phosphate group, each forming an inner-sphere complex with the phosphate oxygens (Fig. 6G). For two Li^+ ions per phosphate group ($N_{Li} = 2$), the DNA charge is exactly reversed. Above this point, the number of adsorbed ions saturates at $\sim N_{Li} = 2.1$. Further ion accumulation is hindered by electrostatic repulsion, which limits the proximity of additional Li^+ ions. Nevertheless, a third Li^+ ion can still bind (Fig. 6G), leading to a saturation level slightly above two ions per phosphate (Fig. 6D).

Finally, the change in twist correlates strongly with the number of specifically adsorbed Li^+ ions (Fig. 6E; Supplementary Table S5). This suggests that in the low salt regime, increased electrostatic screening increases twist and sugar pucker, and decreases radius and rise. In the intermediate salt regime, ion binding slows as the system reaches two

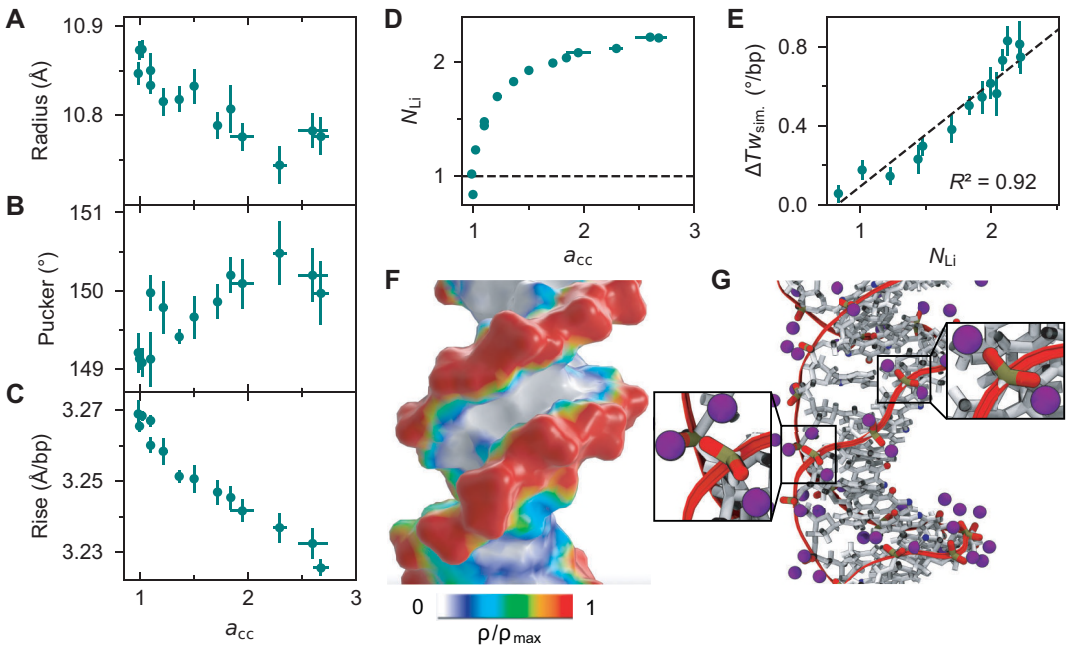

Figure 6. Structural properties of DNA and ion adsorption in the low and high salt regime. Change of structural properties of DNA with increasing activity derivative a_{cc}: (**A**) DNA radius, (**B**) sugar pucker angle, (**C**) helical rise. (**D**) Number of inner-sphere Li^+ ions per phosphate group N_{Li} as a function of the activity derivative a_{cc} using the a_{cc}–concentration relationship from Fig. 5A. The dashed line indicates neutralization of the negative phosphate charge. (**E**) Change in twist from simulations $\Delta T w_{sim}$ as a function of N_{Li}. (**F**) Three-dimensional ion distributions projected on the DNA surface. (**G**) Simulation snapshot illustrating the Li^+ ions (purple) within 3 Å of the non-bridging oxygen atoms of DNA from simulations at 4.4 M LiCl concentration. Zoom-in on selected Li^+-binding sites: two Li^+ ions in inner-sphere configuration with the phosphate oxygens in the upper right and three Li^+ ions per phosphate group in the lower left. All simulations were done with the parmbsc1/Mamatkulov–Schwierz force fields. Data points in (A–E) correspond to the mean ± SEM from six independent simulation runs, except for the activity derivative, where the data are from three independent simulations.

Li^+ ions per phosphate group, and hence the changes in twist and helical properties slow down accordingly. Finally, the onset of the ion adsorption plateau coincides with the saturation of twist, suggesting that high-affinity Li^+ binding is limited by electrostatic repulsion between the cations, which in turn defines an upper bound for DNA twist.

Discussion

Our results demonstrate that the increase in DNA twist with increasing salt concentration, previously documented at lower concentrations, persists well beyond 1 M for all tested monovalent ions, LiCl, NaCl, KCl, and CsCl. This increase in DNA twist, as evidenced by shifts in MT rotation curves, reaches saturation between 4 and 5 M (Fig. 1G).

Notably, the ion-specific differences in DNA twist observed at lower concentrations persist even at the highest salt levels tested, and the twist values at the maximum ΔTw at ∼4 M concentration follow the same trend: $Li^+ > Cs^+ > K^+ > Na^+$. Interestingly, we observe a decrease in twist with increasing salt concentration for the highest concentrations of LiCl and CsCl, at least qualitatively similar to trends in force stability and melting temperature previously attributed to DNA overcharging [2, 79].

To complement the MT measurements, we performed all-atom MD simulations, focusing on LiCl, which produced the largest experimental change in DNA twist. Using selected force fields (parmbsc1 for DNA, the Mamatkulov–Schwierz model for ions, and TIP3P for water), the simulations qualitatively reproduce the twist increase up to high ion concentrations. In contrast, other combinations of DNA and solvent force fields exhibit notable shortcomings in capturing the experimental trends.

While the simulations qualitatively reproduce the twist increase, they systematically underestimate the ion activity and its derivative above ∼2.5 M, suggesting that they overestimate the Li^+–Cl^- (and similarly Na^+–Cl^-) interactions. We find that comparing simulations and experiments using activity derivatives rather than concentrations significantly improves the agreement, capturing both the non-linear twist increase and its saturation (Fig. 5B). This highlights the critical importance of accurately modeling ion–ion and ion–water interactions at high salt concentrations, where standard force fields are typically not optimized. For instance, an activity derivative of ∼2.7, corresponding to 4–5 M LiCl experimentally, reveals a 2-fold discrepancy between simulated and experimental activity derivatives. Improving force field accuracy will require refinement of ion–ion, ion–water, and ion–DNA interactions, specifically through optimizing the cation–anion combination rules at high salt based on experimental data [94–96]. We anticipate that the refinement of force fields will be similarly or even more relevant for simulations with other ions at high concentrations, as for NaCl we found even larger discrepancies between experiments and simulations (Supplementary Fig. S25).

Our results directly address the question of whether C-form DNA exists at high salt concentrations in free solution: notably, we do not observe a shift of ∼2° bp^{-1} twist increase relative to low salt that has been reported for C-form DNA in fiber diffraction studies. Instead, our measurements reveal a maximal twist increase of only ∼0.8° bp^{-1}, which is consistent, within error, with previous ultracentrifugation measurements in 6.2 M LiCl [35]. These experimental findings are

fully corroborated by our MD simulations, which reproduce the observed increases of twist but likewise show no evidence for the C-form in solution even at high salt concentrations. Instead, simulations initiated in either canonical B-form or C-form rapidly converge to B-form, with twist values matching experimental data. While different DNA constructs were used for single-molecule, bulk, and computational experiments due to the specific requirements of each technique, the heterogeneous, "random" sequences used in our assays are considered representative of generic DNA sequences. Therefore, together, our findings suggest that in aqueous solution, even at very high monovalent salt concentrations, DNA with genomic or random sequences remains in the B-form and does not adopt the C-form.

Previously, continuous changes in CD spectra at increasing salt concentrations were interpreted as evidence for the presence of C-form DNA in solution. Our CD spectra are in excellent agreement with these earlier reports. Notably, changes in the band around 280 nm up to 4–5 M concentrations of monovalent alkali ions closely correlate with the increase in DNA twist observed directly by MT and reproduced in our MD simulations. Interestingly, however, both our data and previously published CD spectra show continued spectral shifts at 280 nm even beyond 4–5 M salt, a regime in which the DNA twist, as measured by MT, has already reached its maximum.

The fact that $\Delta\epsilon$ at 280 nm undergoes further changes at salt concentrations where the twist has plateaued and remains constant or decreases implies that CD does not directly report on DNA helical twist. It is currently unclear precisely what molecular features contribute to this aspect of the CD spectra. One possibility are the continued changes in the ion binding pattern including the increasing number of Li^+ ions bound to the nucleobases (Supplementary Fig. S26).

In this context, a promising direction for future research is the development of computational approaches capable of predicting CD spectra directly from MD-generated DNA structures. For proteins, approximate knowledge-based tools such as SESCA [97] or DiChroCalc [98] are already available. For DNA and other systems less well characterized by CD, however, more rigorous first-principles methods such as time-dependent density functional theory or exciton coupling models are likely to be required [99, 100]. In addition, a complementary future direction would be to employ other—ideally high resolution—structural probes of DNA conformations and dynamics, for example Förster resonance energy transfer (FRET) [101–104], (anomalous) X-ray scattering interference [105–107], or nuclear magnetic resonance (NMR) spectroscopy [108, 109], to further experimentally probe DNA structure in solution at very high ionic strengths.

In summary, our data quantitatively describe how DNA twist responds to very high salt concentrations and provide a critical test of molecular force fields in this previously unexplored regime. They offer a robust experimental benchmark for validating simulations and establish a baseline for modeling DNA at extreme ionic conditions, with implications for understanding nucleic acid behavior in extremophiles and prebiotic environments.

Acknowledgements

We thank Alexey Mazur for alerting us to the question of C-DNA formation at high LiCl concentrations and for useful discussions, Dave van den Heuvel, Elleke van Harten, Maria Kurilova, Sidonie Lieber, Andreas Spörhase, and Olga Ustinov for laboratory support, Eefjan Breuking and Christian Kaiser for support with CD measurements, and Gerhard Blab and Martin Zacharias for fruitful discussions.

Author contributions: Koen R. Storm (Conceptualization [equal],Investigation [equal], Methodology [equal], Visualization [equal], Writing – original draft [equal]), Christian Wiebeler (Investigation [equal], Methodology [equal], Visualization [equal], Writing – original draft [equal]), Sergio Cruz-León (Investigation [supporting], Methodology [supporting], Writing – review & editing [equal]), Caroline Körösy (Investigation [supporting], Methodology [supporting], Writing – review & editing [equal]), Nadine Schwierz (Conceptualization [equal], Funding acquisition [equal], Supervision [equal], Writing – review & editing [equal]), Jan Lipfert (Conceptualization [equal], Funding acquisition [equal], Project administration [equal], Supervision [equal], Writing – original draft [equal]).

Supplementary data

Supplementary data is available at NAR online.

Conflict of interest

None declared.

Funding

Utrecht University; the European Research Council [Consolidator Grant "ProForce" 101002656]; Erlangen National High Performance Computing Center (NHR@FAU) of the Friedrich-Alexander-Universität Erlangen-Nürnberg (FAU) [b119ee and b253ee]; and the LiCCA HPC cluster of the University of Augsburg, co-funded by the Deutsche Forschungsgemeinschaft [499211671].

Data availability

The data underlying this article are freely available in the Zenodo repository at https://doi.org/10.5281/zenodo.17093172.

References

1. Lipfert J, Doniach S, Das R *et al.* Understanding nucleic acid–ion interactions. *Annu Rev Biochem* 2014;83:813–41. https://doi.org/10.1146/annurev-biochem-060409-092720
2. Zhang C, Tian FJ, Zuo HW *et al.* Counterintuitive DNA destabilization by monovalent salt at high concentrations due to overcharging. *Nat Commun* 2025;16:113. https://doi.org/10.1038/s41467-024-55404-6
3. Watson JD, Crick FH. Molecular structure of nucleic acids. *Nature* 1953;171:737–8. https://doi.org/10.1038/171737a0
4. Anderson P, Bauer W. Supercoiling in closed circular DNA: dependence upon ion type and concentration. *Biochemistry* 1978;17:594–601. https://doi.org/10.1021/bi00597a006
5. Xu YC, Bremer H. Winding of the DNA helix by divalent metal ions. *Nucleic Acids Res* 1997;25:4067–71. https://doi.org/10.1093/nar/25.20.4067
6. Cruz-León S, Vanderlinden W, Müller P *et al.* Twisting DNA by salt. *Nucleic Acids Res* 2022;50:5726–38. https://doi.org/10.1093/nar/gkac445
7. Tian FJ, Zhang C, Zhou E *et al.* Universality in RNA and DNA deformations induced by salt, temperature change, stretching

force, and protein binding. *Proc Natl Acad Sci USA* 2023;120:e2218425120. https://doi.org/10.1073/pnas.2218425120
8. Zhang C, Tian F, Lu Y *et al.* Twist–diameter coupling drives DNA twist changes with salt and temperature. *Sci Adv* 2022;8:eabn1384. https://doi.org/10.1126/sciadv.abn1384
9. Robinson RA. The water activities of lithium chloride solutions up to high concentrations at 25°. *Trans Faraday Soc* 1945;41:756–8. https://doi.org/10.1039/TF9454100756
10. Oren A. Life at high salt concentrations. In:Rosenberg E, DeLong EF, Lory S, Stackebrandt E, Thompson F (eds.), *The Prokaryotes: Prokaryotic Communities and Ecophysiology*. Berlin, Heidelberg: Springer, 2013, 421–40.
11. Corral P, Amoozegar MA, Ventosa A. Halophiles and their biomolecules: recent advances and future applications in biomedicine. *Mar Drugs* 2020;18:33. https://doi.org/10.3390/md18010033
12. Oren A. Novel insights into the diversity of halophilic microorganisms and their functioning in hypersaline ecosystems. *NPJ Biodivers* 2024;3:18. https://doi.org/10.1038/s44185-024-00050-w
13. van Zelm E, Zhang Y, Testerink C. Salt tolerance mechanisms of plants. *Annu Rev Plant Biol* 2020;71:403–33. https://doi.org/10.1146/annurev-arplant-050718-100005
14. Yi R, Hongo Y, Yoda I *et al.* Radiolytic synthesis of cyanogen chloride, cyanamide and simple sugar precursors. *ChemistrySelect* 2018;3:10169–74. https://doi.org/10.1002/slct.201802242
15. do Nascimento Vieira A, Kleinermanns K, Martin WF *et al.* The ambivalent role of water at the origins of life. *FEBS Lett* 2020;594:2717–33. https://doi.org/10.1002/1873-3468.13815
16. Matreux T, Le Vay K, Schmid A *et al.* Heat flows in rock cracks naturally optimize salt compositions for ribozymes. *Nat Chem* 2021;13:1038–45. https://doi.org/10.1038/s41557-021-00772-5
17. Ginter T, Dujardin A, Roumans S *et al.* Environmental constraints on the origin of life based on membrane formation: the role of salinity. *Int J Astrobiol* 2024;23:e25. https://doi.org/10.1017/S147355042400020X
18. Cruz-León S, Schwierz N. Hofmeister series for metal-cation–RNA interactions: the interplay of binding affinity and exchange kinetics. *Langmuir* 2020;36:5979–89. https://doi.org/10.1021/acs.langmuir.0c00851
19. Dong H-L, Zhang C, Dai L *et al.* The origin of different bending stiffness between double-stranded RNA and DNA revealed by magnetic tweezers and simulations. *Nucleic Acids Res* 2024;52:2519–29. https://doi.org/10.1093/nar/gkae063
20. Langridge R, Seeds WE, Wilson HR *et al.* Molecular structure of deoxyribonucleic acid (DNA). *J Biophys Biochem Cytol* 1957;3:767–78. https://doi.org/10.1083/jcb.3.5.767
21. Marvin DA, Spencer M, Wilkins MHF *et al.* A new configuration of deoxyribonucleic acid. *Nature* 1958;182:387–8. https://doi.org/10.1038/182387b0
22. Hamilton LD. DNA: models and reality. *Nature* 1968;218:633–7. https://doi.org/10.1038/218633a0
23. Marvin DA, Spencer M, Wilkins MH *et al.* The molecular configuration of deoxyribonucleic acid. III. X-ray diffraction study of the C form of the lithium salt. *J Mol Biol* 1961;3:547–65. https://doi.org/10.1016/S0022-2836(61)80021-1
24. Arnott S, Selsing E. The conformation of C-DNA. *J Mol Biol* 1975;98:265–9. https://doi.org/10.1016/S0022-2836(75)80115-X
25. Portugal J, Subirana JA. Counterions which favour the C form of DNA. *EMBO J* 1985;4:2403–8. https://doi.org/10.1002/j.1460-2075.1985.tb03946.x
26. Lu XJ, Olson WK. 3DNA: a software package for the analysis, rebuilding and visualization of three-dimensional nucleic acid structures. *Nucleic Acids Res* 2003;31:5108–21. https://doi.org/10.1093/nar/gkg680
27. Egli M. Flavell A, Pyle AM *et al.* DNA and RNA structure. In: Blackburn GM, Egli M, Gait MJ, Watts JK (eds.), *Nucleic Acids in Chemistry and Biology*. London: The Royal Society of Chemistry, 2022, 13–76.
28. Mazur AK, Gladyshev E. C-DNA may facilitate homologous DNA pairing. *Trends Genet* 2023;39:575–85. https://doi.org/10.1016/j.tig.2023.01.008
29. Strelnikov IA, Kovaleva NA, Klinov AP *et al.* C–B–A test of DNA force fields. *ACS Omega* 2023;8:10253–65. https://doi.org/10.1021/acsomega.2c07781
30. Liebl K, Zacharias M. Tumuc1: a new accurate DNA force field consistent with high-level quantum chemistry. *J Chem Theory Comput* 2021;17:7096–105. https://doi.org/10.1021/acs.jctc.1c00682
31. Hanlon S, Brudno S, Wu TT *et al.* Structural transitions of deoxyribonucleic acid in aqueous electrolyte solutions. I. Reference spectra of conformational limits. *Biochemistry* 1975;14:1648–60. https://doi.org/10.1021/bi00679a017
32. Hanlon S, Johnson RS, Wolf B *et al.* Mixed conformations of deoxyribonucleic acid in chromatin: a preliminary report. *Proc Natl Acad Sci USA* 1972;69:3263–7. https://doi.org/10.1073/pnas.69.11.3263
33. Tunis-Schneider MJB, Maestre MF. Circular dichroism spectra of oriented and unoriented deoxyribonucleic acid films—a preliminary study. *J Mol Biol* 1970;52:521–41. https://doi.org/10.1016/0022-2836(70)90417-1
34. Ivanov VI, Minchenkova LE, Schyolkina AK *et al.* Different conformations of double-stranded nucleic acid in solution as revealed by circular dichroism. *Biopolymers* 1973;12:89–110. https://doi.org/10.1002/bip.1973.360120109
35. Baase WA, Johnson WC, Jr. Circular dichroism and DNA secondary structure. *Nucleic Acids Res* 1979;6:797–814. https://doi.org/10.1093/nar/6.2.797
36. Zimmerman SB, Pheiffer BH. Does DNA adopt the C form in concentrated salt solutions or in organic solvent/water mixtures? An X-ray diffraction study of DNA fibers immersed in various media. *J Mol Biol* 1980;142:315–30. https://doi.org/10.1016/0022-2836(80)90275-2
37. Mazur AK, Maaloum M, Gladyshev E. Properties of DNA in concentrated aqueous solutions of LiCl suggest transition to C-DNA. *bioRxiv* 2024; 2024.2009.2020.613475, 23 September 2024, preprint: not peer reviewed .
38. Hart K, Foloppe N, Baker CM *et al.* Optimization of the CHARMM additive force field for DNA: improved treatment of the BI/BII conformational equilibrium. *J Chem Theory Comput* 2012;8:348–62. https://doi.org/10.1021/ct200723y
39. Zgarbová M, Šponer J, Jurečka P. Z-DNA as a touchstone for additive empirical force fields and a refinement of the alpha/gamma DNA torsions for AMBER. *J Chem Theory Comput* 2021;17:6292–301. https://doi.org/10.1021/acs.jctc.1c00697
40. Ivani I, Dans PD, Noy A *et al.* Parmbsc1: a refined force field for DNA simulations. *Nat Methods* 2016;13:55–8. https://doi.org/10.1038/nmeth.3658
41. Haynes WM. *CRC Handbook of Chemistry and Physics*. Boca Raton, FL: CRC Press, 2014.
42. Lipfert J, Koster DA, Vilfan ID *et al.* Single-molecule magnetic tweezers studies of type IB topoisomerases. *Methods Mol Biol* 2009;582:71–89. https://doi.org/10.1007/978-1-60761-340-4_7
43. Lipfert J, Klijnhout S, Dekker NH. Torsional sensing of small-molecule binding using magnetic tweezers. *Nucleic Acids Res* 2010;38:7122–32. https://doi.org/10.1093/nar/gkq598
44. Lipfert J, Kerssemakers JW, Jager T *et al.* Magnetic torque tweezers: measuring torsional stiffness in DNA and RecA–DNA filaments. *Nat Methods* 2010;7:977–80. https://doi.org/10.1038/nmeth.1520
45. Kriegel F, Vanderlinden W, Nicolaus T *et al.* Measuring single-molecule twist and torque in multiplexed magnetic

tweezers. *Methods Mol Biol* 2018;1814:75–98. https://doi.org/10.1007/978-1-4939-8591-3_6.
46. Walker PU, Vanderlinden W, Lipfert J. Dynamics and energy landscape of DNA plectoneme nucleation. *Phys Rev E* 2018;98:042412. https://doi.org/10.1103/PhysRevE.98.042412
47. Lipfert J, Hao X, Dekker NH. Quantitative modeling and optimization of magnetic tweezers. *Biophys J* 2009;96:5040–9. https://doi.org/10.1016/j.bpj.2009.03.055
48. van Loenhout MT, Kerssemakers JW, De Vlaminck I *et al.* Non-bias-limited tracking of spherical particles, enabling nanometer resolution at low magnification. *Biophys J* 2012;102:2362–71. https://doi.org/10.1016/j.bpj.2012.03.073
49. Cnossen JP, Dulin D, Dekker NH. An optimized software framework for real-time, high-throughput tracking of spherical beads. *Rev Sci Instrum* 2014;85:103712. https://doi.org/10.1063/1.4898178
50. Velthuis A, Kerssemakers JWJ, Lipfert J *et al.* Quantitative guidelines for force calibration through spectral analysis of magnetic tweezers data. *Biophys J* 2010;99:1292–302. https://doi.org/10.1016/j.bpj.2010.06.008
51. Pritzl SD, Ulugöl A, Körösy C *et al.* Accurate drift-invariant single-molecule force calibration using the Hadamard variance. *Biophys J* 2024;123:3964–76. https://doi.org/10.1016/j.bpj.2024.10.008
52. De Vlaminck I, Henighan T, van Loenhout MT *et al.* Magnetic forces and DNA mechanics in multiplexed magnetic tweezers. *PLoS One* 2012;7:e41432. https://doi.org/10.1371/journal.pone.0041432
53. Lof A, Walker PU, Sedlak SM *et al.* Multiplexed protein force spectroscopy reveals equilibrium protein folding dynamics and the low-force response of von Willebrand factor. *Proc Natl Acad Sci USA* 2019;116:18798–807. https://doi.org/10.1073/pnas.1901794116
54. Strick TR, Croquette V, Bensimon D. Homologous pairing in stretched supercoiled DNA. *Proc Natl Acad Sci USA* 1998;95:10579–83. https://doi.org/10.1073/pnas.95.18.10579
55. Klaue D, Seidel R. Torsional stiffness of single superparamagnetic microspheres in an external magnetic field. *Phys Rev Lett* 2009;102:028302. https://doi.org/10.1103/PhysRevLett.102.028302
56. Daldrop P, Brutzer H, Huhle A *et al.* Extending the range for force calibration in magnetic tweezers. *Biophys J* 2015;108:2550–61. https://doi.org/10.1016/j.bpj.2015.04.011
57. Abraham MJ, Murtola T, Schulz R *et al.* GROMACS: high performance molecular simulations through multi-level parallelism from laptops to supercomputers. *SoftwareX* 2015;1-2:19–25. https://doi.org/10.1016/j.softx.2015.06.001
58. Li S, Olson WK, Lu X-J. Web 3DNA 2.0 for the analysis, visualization, and modeling of 3D nucleic acid structures. *Nucleic Acids Res* 2019;47:W26–34. https://doi.org/10.1093/nar/gkz394
59. Mamatkulov S, Schwierz N. Force fields for monovalent and divalent metal cations in TIP3P water based on thermodynamic and kinetic properties. *J Chem Phys* 2018;148:074504. https://doi.org/10.1063/1.5017694
60. Jorgensen WL, Chandrasekhar J, Madura JD *et al.* Comparison of simple potential functions for simulating liquid water. *J Chem Phys* 1983;79:926–35. https://doi.org/10.1063/1.445869
61. Kirkwood JG, Buff FP. The statistical mechanical theory of solutions. I. *J Chem Phys* 1951;19:774–7. https://doi.org/10.1063/1.1748352
62. Weerasinghe S, Smith PE. A Kirkwood–Buff derived force field for sodium chloride in water. *J Chem Phys* 2003;119:11342–9. https://doi.org/10.1063/1.1622372
63. Joung IS, Cheatham TE, 3rd. Determination of alkali and halide monovalent ion parameters for use in explicitly solvated biomolecular simulations. *J Phys Chem B* 2008;112:9020–41. https://doi.org/10.1021/jp8001614
64. Horn HW, Swope WC, Pitera JW *et al.* Development of an improved four-site water model for biomolecular simulations: tIP4P-Ew. *J Chem Phys* 2004;120:9665–78. https://doi.org/10.1063/1.1683075
65. Bussi G, Donadio D, Parrinello M. Canonical sampling through velocity rescaling. *J Chem Phys* 2007;126:014101. https://doi.org/10.1063/1.2408420
66. Parrinello M, Rahman A. Polymorphic transitions in single crystals: a new molecular dynamics method. *J Appl Phys* 1981;52:7182–90. https://doi.org/10.1063/1.328693
67. Lu X-J, Olson WK. 3DNA: a versatile, integrated software system for the analysis, rebuilding and visualization of three-dimensional nucleic-acid structures. *Nat Protoc* 2008;3:1213–27. https://doi.org/10.1038/nprot.2008.104
68. Kumar R, Grubmüller H. do_x3dna: a tool to analyze structural fluctuations of dsDNA or dsRNA from molecular dynamics simulations. *Bioinformatics* 2015;31:2583–5. https://doi.org/10.1093/bioinformatics/btv190
69. Daura X, Gademann K, Jaun B *et al.* Peptide folding: when simulation meets experiment. *Angew Chem Int Ed* 1999;38:236–40. https://doi.org/10.1002/(SICI)1521-3773(19990115)38:1/2⟨236::AID-ANIE236⟩3.0.CO;2-M
70. Briones R, Blau C, Kutzner C *et al.* GROMaps: a GROMACS-based toolset to analyze density maps derived from molecular dynamics simulations. *Biophys J* 2019;116:4–11. https://doi.org/10.1016/j.bpj.2018.11.3126
71. Strick TR, Allemand JF, Bensimon D *et al.* The elasticity of a single supercoiled DNA molecule. *Science* 1996;271:1835–7. https://doi.org/10.1126/science.271.5257.1835
72. Ritort F. Single-molecule experiments in biological physics: methods and applications. *J Phys: Condens Matter* 2006;18:R531–83. https://doi.org/10.1088/0953-8984/18/32/R01
73. Neuman KC, Nagy A. Single-molecule force spectroscopy: optical tweezers, magnetic tweezers and atomic force microscopy. *Nat Methods* 2008;5:491–505. https://doi.org/10.1038/nmeth.1218
74. Vilfan ID, Lipfert J, Koster DA *et al.* Magnetic tweezers for single-molecule experiments. In: Hinterdorfer P, van Oijen A. (eds), *Handbook of Single-Molecule Biophysics*. New York: Springer, 2009, 371–95.
75. Bustamante C, Marko JF, Siggia ED *et al.* Entropic elasticity of lambda-phage DNA. *Science* 1994;265:1599–600. https://doi.org/10.1126/science.8079175
76. Bustamante C, Bryant Z, Smith SB. Ten years of tension: single-molecule DNA mechanics. *Nature* 2003;421:423–7. https://doi.org/10.1038/nature01405
77. Kriegel F, Ermann N, Lipfert J. Probing the mechanical properties, conformational changes, and interactions of nucleic acids with magnetic tweezers. *J Struct Biol* 2017;197:26–36. https://doi.org/10.1016/j.jsb.2016.06.022
78. Kriegel F, Matek C, Drsata T *et al.* The temperature dependence of the helical twist of DNA. *Nucleic Acids Res* 2018;46:7998–8009. https://doi.org/10.1093/nar/gky599
79. Wei W, Tian F-J, Chen Z-X *et al.* Charge inversion of single-stranded DNA under high-concentration monovalent salts. *Macromolecules* 2025;58:12882–92, https://doi.org/10.1021/acs.macromol.5c02249
80. Clauvelin N, Audoly B, Neukirch S. Elasticity and electrostatics of plectonemic DNA. *Biophys J* 2009;96:3716–23. https://doi.org/10.1016/j.bpj.2009.02.032
81. Neukirch S, Marko JF. Analytical description of extension, torque, and supercoiling radius of a stretched twisted DNA. *Phys Rev Lett* 2011;106:138104. https://doi.org/10.1103/PhysRevLett.106.138104
82. Mosconi F, Allemand JF, Bensimon D *et al.* Measurement of the torque on a single stretched and twisted DNA using magnetic tweezers. *Phys Rev Lett* 2009;102:078301. https://doi.org/10.1103/PhysRevLett.102.078301
83. Maffeo C, Schopflin R, Brutzer H *et al.* DNA–DNA interactions in tight supercoils are described by a small effective charge

density. *Phys Rev Lett* 2010;105:158101. https://doi.org/10.1103/PhysRevLett.105.158101
84. Das U, Magateshvaren Saras MA, Rathinavelan T. NuCDB: a databank of nucleic acids circular dichroism spectra. bioRxiv, https://doi.org/10.1101/2024.04.19.590190, 22 April 2024, preprint: not peer reviewed.
85. Segel DJ, Fink AL, Hodgson KO *et al.* Protein denaturation: a small-angle X-ray scattering study of the ensemble of unfolded states of cytochrome c. *Biochemistry* 1998;37:12443–51. https://doi.org/10.1021/bi980535t
86. Doniach S. Changes in biomolecular conformation seen by small angle X-ray scattering. *Chem Rev* 2001;101:1763–78. https://doi.org/10.1021/cr990071k
87. Russell R, Millett IS, Tate MW *et al.* Rapid compaction during RNA folding. *Proc Natl Acad Sci USA* 2002;99:4266–71. https://doi.org/10.1073/pnas.072589599
88. Liebl K, Drsata T, Lankas F *et al.* Explaining the striking difference in twist–stretch coupling between DNA and RNA: a comparative molecular dynamics analysis. *Nucleic Acids Res* 2015;43:10143–56.
89. Dohnalová H, Seifert M, Matoušková E *et al.* Temperature-dependent twist of double-stranded RNA probed by magnetic tweezer experiments and molecular dynamics simulations. *J Phys Chem B* 2024;128:664–75. https://doi.org/10.1021/acs.jpcb.3c06280
90. Lavery R, Zakrzewska K, Beveridge D *et al.* A systematic molecular dynamics study of nearest-neighbor effects on base pair and base pair step conformations and fluctuations in B-DNA. *Nucleic Acids Res* 2009;38:299–313. https://doi.org/10.1093/nar/gkp834
91. Dans PD, Faustino I, Battistini F *et al.* Unraveling the sequence-dependent polymorphic behavior of d(CpG) steps in B-DNA. *Nucleic Acids Res* 2014;42:11304–20. https://doi.org/10.1093/nar/gku809
92. Zgarbová M, Jurečka P, Lankaš F *et al.* Influence of BII backbone substates on DNA twist: a unified view and comparison of simulation and experiment for all 136 distinct tetranucleotide sequences. *J Chem Inf Model* 2017;57:275–87. https://doi.org/10.1021/acs.jcim.6b00621
93. van Dam L, Levitt MH. BII nucleotides in the B and C forms of natural-sequence polymeric DNA: a new model for the C form of DNA. *J Mol Biol* 2000;304:541–61. https://doi.org/10.1006/jmbi.2000.4194
94. Fyta M, Netz RR. Ionic force field optimization based on single-ion and ion-pair solvation properties: going beyond standard mixing rules. *J Chem Phys* 2012;136:12410. https://doi.org/10.1063/1.3693330
95. Mamatkulov S, Fyta M, Netz RR. Force fields for divalent cations based on single-ion and ion-pair properties. *J Chem Phys* 2013;138:024505. https://doi.org/10.1063/1.4772808
96. Cruz-León S, Grotz KK, Schwierz N. Extended magnesium and calcium force field parameters for accurate ion–nucleic acid interactions in biomolecular simulations. *J Chem Phys* 2021;154:171102. https://doi.org/10.1063/5.0048113
97. Nagy G, Igaev M, Jones NC *et al.* SESCA: predicting circular dichroism spectra from protein molecular structures. *J Chem Theory Comput* 2019;15:5087–102. https://doi.org/10.1021/acs.jctc.9b00203
98. Bulheller BM, Hirst JD. DichroCalc—circular and linear dichroism online. *Bioinformatics* 2009;25:539–40. https://doi.org/10.1093/bioinformatics/btp016
99. Miyahara T, Nakatsuji H, Sugiyama H. Similarities and differences between RNA and DNA double-helical structures in circular dichroism spectroscopy: a SAC–CI study. *J Phys Chem A* 2016;120:9008–18. https://doi.org/10.1021/acs.jpca.6b08023
100. Seibert J, Bannwarth C, Grimme S. Biomolecular structure information from high-speed quantum mechanical electronic spectra calculation. *J Am Chem Soc* 2017;139:11682–5. https://doi.org/10.1021/jacs.7b05833
101. Clegg RM, Murchie AI, Zechel A *et al.* Observing the helical geometry of double-stranded DNA in solution by fluorescence resonance energy transfer. *Proc Natl Acad Sci USA* 1993;90:2994–8. https://doi.org/10.1073/pnas.90.7.2994
102. Iqbal A, Arslan S, Okumus B *et al.* Orientation dependence in fluorescent energy transfer between Cy3 and Cy5 terminally attached to double-stranded nucleic acids. *Proc Natl Acad Sci USA* 2008;105:11176–81. https://doi.org/10.1073/pnas.0801707105
103. Hellenkamp B, Schmid S, Doroshenko O *et al.* Precision and accuracy of single-molecule FRET measurements—a multi-laboratory benchmark study. *Nat Methods* 2018;15:669–76. https://doi.org/10.1038/s41592-018-0085-0
104. Lerner E, Cordes T, Ingargiola A *et al.* Toward dynamic structural biology: two decades of single-molecule Förster resonance energy transfer. *Science* 2018;359:eaan1133. https://doi.org/10.1126/science.aan1133
105. Mathew-Fenn RS, Das R, Harbury PA. Remeasuring the double helix. *Science* 2008;322:446–9. https://doi.org/10.1126/science.1158881
106. Shi X, Beauchamp KA, Harbury PB *et al.* From a structural average to the conformational ensemble of a DNA bulge. *Proc Natl Acad Sci USA* 2014;111:E1473–80. https://doi.org/10.1073/pnas.1317032111
107. Zettl T, Mathew RS, Seifert S *et al.* Absolute intramolecular distance measurements with Angstrom-resolution using anomalous small-angle X-ray scattering. *Nano Lett* 2016;16:5353–7. https://doi.org/10.1021/acs.nanolett.6b01160
108. Wijmenga SS, van Buuren BNM. The use of NMR methods for conformational studies of nucleic acids. *Prog Nucl Magn Reson Spectrosc* 1998;32:287–387. https://doi.org/10.1016/S0079-6565(97)00023-X
109. Nikolova EN, Kim E, Wise AA *et al.* Transient Hoogsteen base pairs in canonical duplex DNA. *Nature* 2011;470:498–502. https://doi.org/10.1038/nature09775
110. Hamer WJ, Wu YC. Osmotic coefficients and mean activity coefficients of uni-univalent electrolytes in water at 25°C. *J Phys Chem Ref Data* 1972;1:1047–100. https://doi.org/10.1063/1.3253108

Received: September 15, 2025. **Revised:** January 24, 2026. **Accepted:** February 16, 2026